Design of Pivot less Tilting Pad Journal Bearing for Cryogenic Turboexpander

Sonal Kumar, Rajiv Ranjan, Subrata K. Ghosh*
Department of ME & MME, ISM, Dhanbad, Jharkhand, India

*Corresponding author (email: subratarec@yahoo.co.in)

Abstract

The research presented in this paper is aimed at the design of Tilting pad journal bearing. This bearing generally consists of three pads pivoted with bearing housing. This paper provides method for simulation of the pressure distribution inside the bearing. The modulation of the back face pressure is done by the aerodynamic pressure developed in the clearance space between the rotor and the pad through the connecting holes and bleed hole. The pressure distribution of the gas film within the bearing is governed by Reynolds equation which is distinct solution by finite difference method. Initially computation of the geometry of the pad is done followed by the determination of pressure distribution with the help of MATLAB Programming.

1. Introduction

Cryogenic turboexpander generally run at very high speed and relatively low loads. It is preferred to use gas-lubricated bearings over oil-lubricated bearings for cryogenic turboexpander [1]. Gas bearings are particularly attractive for using high speed applications because of low viscosity, which results in much lower power losses than occur in their oil lubricated counterparts. Also noteworthy is the increase in gas viscosity with increase in temperature which minimizes thermal issues and may operate at up to 700,000 rpm with no cooling requirements [1 - 2].

Tilting pad journal bearings has got one distinct advantage over the full 360^0 journal bearing that it is almost free from half speed whirling . Pivot-less tilting pad gas journal bearing is invented by Jost and Trepp[3] and used by Sulzer Brothers, Switzerland [4]. The basic journal bearing system is shown in Fig. 1. Since the design methods of these bearings are not available in open literature, this chapter serves to fill in the void and provide a procedure for geometrical design of a pad along with a method for simulation of pressure variation inside the bearing.
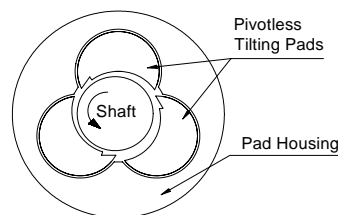

Figure 1: Schematic of a pivotless tilting pad bearing

Nomenclature

R	Shaft radius
r	Pad radius
r_0	Pad housing radius
R_0	Pad housing edge radius
C	Pad clearance with rotor
H_0	Clearance with pad housing
L	Pad length
α'	Total pad angle
α	Effective pad angle
γ	Pad angle ratio
δ	Angular extent of pad trailing edge wedge
D_w	Wedge width
Δ	Wedge depth
θ_3	Effective angular extent of the back face
ξ	Angular location of pad leading edge from the position of maximum film thickness
θ_{incl}	Included angle between connecting holes
d_{con}	Connecting hole diameter
d_{bleed}	Bleed hole diameter

2. Working Principle

Each pad basically consists of a front face that forms the bearing surface, a back face, a network of three holes in one plane with two such planes located symmetrically across the pad length, and a trailing edge wedge is shown in Fig. 2. The wedge, along with the network of holes, forms a system that acts as a replacement for the pad pivot. High pressure from the bearing surface is communicated to the back face of the pad through the holes. This generates a pressure profile at the back face; the force due to that pressure passes through the geometric centre of the circle defining the face. This geometric centre can be regarded as the position of an imaginary pivot that divides the bearing area into two unequal parts due to the presence of the wedge. The forces coming into picture are the aerodynamic load on the pad, the frictional force on the bearing surface and the force due to pressure distribution at the pad back face. The modulation of back face pressure is supposed to be done by the aerodynamic pressure developed in the clearance space between the rotor and the pad. Any rise in bearing pressure at the bleed hole entry, due to increased

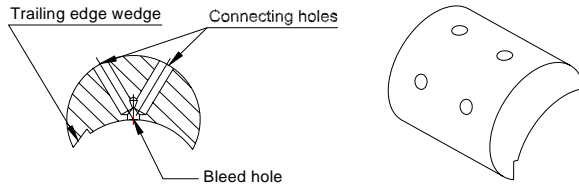external load, triggers an identical response at the back face of the pad.

Figure 2: A single pad with its features

3. Governing Equations

In order to simplify the entire analysis is broken up into two distinct parts. The effective bearing surface along with the rotor is treated as a partial arc bearing while the back face has a pressure distribution solely contributed by aerostatic means.

3.1 The partial arc aerodynamic journal bearing

Considering the pad surface and the rotor as a partial arc bearing, the dimensionless Reynolds equation in steady state can be expressed in the following form [5 - 6]:

$$\frac{\partial}{\partial \theta}\left[PH^3 \frac{\partial P}{\partial \theta}\right]+\left(\frac{R}{L}\right)^2 \frac{\partial}{\partial \eta}\left[PH^3 \frac{\partial P}{\partial \eta}\right]=\Lambda \frac{\partial}{\partial \theta}(PH) \quad (1)$$

where,

$P = p/p_a$ is the dimensionless pressure

p = bearing pressure at any location θ, z

p_a = the ambient pressure

$\eta = z/L$ is the dimensionless location in the axial direction along pad length

θ = angular location around the bearing circumference measured from the position of maximum film thickness,

$$\Lambda = \frac{6\mu\omega}{p_a}\left(\frac{R}{C}\right)^2 \quad (2)$$

Λ being the bearing number and ω the angular velocity of the rotor.

The dimensionless film thickness,

$H = h/C = (1 + \varepsilon \cos\theta)$ \quad (3)

where,

h = Film thickness at any location θ, z

$\varepsilon = e/C$ is the journal eccentricity ratio, and

e = Journal eccentricity

The boundary conditions required for solving equation (1) are:

$$P(\xi,\eta)= P(\xi+\alpha,\eta)=1$$
$$P(\theta, 0)= P(\theta,1)=1 \quad (4)$$

The boundary conditions are the consequence of the fact that the pressure at the edge of the pad is ambient.

3.2 Back face of the pad

The fact that a thin film of gas surrounds the pad back face and separates it from the housing makes it possible to treat the pad-housing combination as a bearing. The Reynolds equation for the bearing is expressed in the form equation (5):

$$\frac{\partial}{\partial \theta}\left[P \overline{H}^3 \frac{\partial P}{\partial \theta}\right]+\left(\frac{r}{L}\right)^2 \frac{\partial}{\partial \eta}\left[P \overline{H}^3 \frac{\partial P}{\partial \eta}\right]=0 \quad (5)$$

where,

$$\overline{H} = \frac{\overline{h}}{H_0}=1-\varepsilon_s \cos\left(\frac{\theta_3}{2}-\theta\right) \quad (6)$$

$\overline{h}$ being the pad back face clearance at any angle θ measured from the edge of the housing is shown in Fig. 3 and ε_s the eccentricity ratio of the pad with respect to the housing.
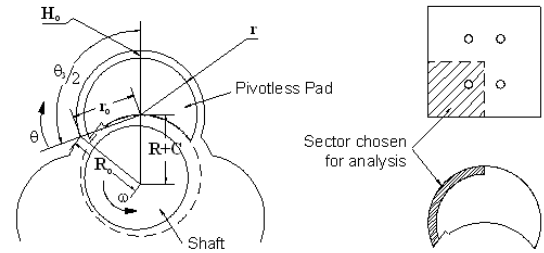

Figure 3: Sector under investigation at the back face of the pad

Due to the symmetrical location of the holes, only one quarter of the back face, having a single gas feed hole, is considered for analysis and computation. The boundary conditions required for solving equation (5) are:

$$\left.\begin{array}{l} P(\theta=0,\eta)= P(\theta,\eta = 0)=1 \\ \dfrac{\partial P}{\partial \theta} = 0\,;\, \theta = \dfrac{\theta_3}{2},\eta \\ \dfrac{\partial P}{\partial \eta} = 0\,;\, \theta, \eta = 0.5 \\ P_{hole} = P_{dyn} \end{array}\right\} \quad (7)$$

The first condition arises from the fact that the pressure at the edges of the pad is ambient. The second and the third conditions are due to the effect of symmetric pressure distribution along the circumferential and axial directions over the pad. The last condition merely states that the pressure at the exit of the gas feed hole P_{hole} is the same as P_{dyn}, the pressure at the entry of bleed hole on the pad-rotor bearing surface.

4. Method of solution

4.1 Computation of pad geometry

The schematic of a single pad and rotor geometry is shown in Fig. 4. With the assumption of pad centre coinciding with the pad front face, the pad back face radius can be approximately expressed as

$$r = 2(R+C)\sin\left(\frac{\alpha'}{4}\right) \qquad (8)$$

The value of r computed from equation (8) is then corrected to nearest meaningful value r_0 from machining considerations. The pad housing radius, r_0 is computed from the relation:

$$r_0 = r_c + H_0 \qquad (9)$$

Now, working backwards, the corrected value of α' is obtained as:

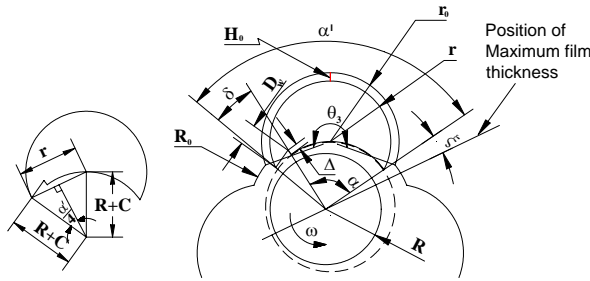$$\alpha'_c = 4\sin^{-1}\left[\frac{r_c}{2(R+C)}\right] \qquad (10)$$

Figure 4: Pad and rotor geometry

The corrected value of α_c' is not far from that of α'. The slot angle δ is now calculated from the relation:

$$\delta = \alpha'_c\left(1 - \frac{1}{\gamma}\right) \qquad (11)$$

The actual wedge width D_w is then computed from the formula:

$$D_w = 2(R+C)\sin\left(\frac{\delta}{2}\right) \qquad (12)$$

The calculated value of D_w can be corrected to the nearest meaningful number D_c from considerations of pad machining constraints. The modified value of slot angle, δ_c is then determined by working backwards:

$$\delta_c = 2\sin^{-1}\left[\frac{D_c}{2(R+C)}\right] \qquad (13)$$

Using equations (11) and (13) the modified value of γ_r is found as:

$$\gamma_r = \frac{\alpha'_c}{\alpha'_c - \delta_c} \qquad (14)$$

Once the pad angle ratio is fixed, it is possible to determine the angular extent of the effective pad arc from the relation:

$$\alpha = \frac{\alpha'_c}{\gamma_r} \qquad (15)$$

The angular location of the imaginary pivot is then determined from the formula:

$$\phi = \frac{\alpha'_c/2}{\alpha} \qquad (16)$$

Using trigonometry, the angular extent of clearance between pad back face and housing is calculated from Fig.5.

$$\theta_3 = 2(\theta_1 + \theta_2) \qquad (17)$$

where,

$$\theta_1 = \cos^{-1}\left[\frac{(R_0^2 - r_0^2) + (R+C)^2}{2R_0(R+C)}\right] \qquad (18)$$

$$\theta_2 = \sin^{-1}\left[\left(\frac{R+C}{r_0}\right)\sin\theta_1\right] \qquad (19)$$
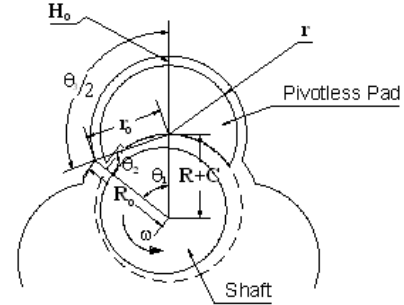

Figure 5: Geometrical relationship between pad and housing features

4.2 Numerical Scheme

4.2.1 The partial arc aerodynamic journal bearing

In order to obtain the pressure at the bearing clearance, equation (1) has to be solved numerically. The finite difference method is employed for the purpose. Equation (1) is discritised for solution by FDM [7] and expressed in the following form:

$$P_{i,j}^2 - 2E_{i,j}P_{i,j} + F_{i,j} = 0 \qquad (20)$$

where,
i and j are grid locations in θ and η directions respectively.

$$E_{i,j} = \frac{(P_{i+1,j}+P_{i-1,j})}{2\overline{D}(\Delta\theta)^2} + \frac{3}{4\overline{D}H_i(\Delta\theta)}\frac{dH}{d\theta}\bigg|_i (P_{i+1,j}-P_{i-1,j})$$
$$+ \left(\frac{R}{L}\right)^2\frac{(P_{i,j+1}+P_{i,j-1})}{2\overline{D}(\Delta\eta)^2} - \frac{\Lambda}{2\overline{D}H_i^3}\frac{dH}{d\theta}\bigg|_i \qquad (21)$$

$$F_{i,j} = \frac{\Lambda(P_{i+1,j}-P_{i-1,j})}{2\overline{D}H_i^2(\Delta\theta)} - \frac{(P_{i+1,j}-P_{i-1,j})^2}{4\overline{D}(\Delta\theta)^2} - \left(\frac{R}{L}\right)^2\frac{(P_{i,j+1}-P_{i,j-1})^2}{4\overline{D}(\Delta\eta)^2} \qquad (22)$$

$$\Delta\theta = \frac{\alpha}{M} \qquad (23)$$

$$\Delta\eta = \frac{1}{N} \qquad (24)$$

$$\overline{D} = 2\left[\frac{1}{(\Delta\theta)^2} + \left(\frac{R}{L}\right)^2\frac{1}{(\Delta\eta)^2}\right] \qquad (25)$$

$$H_i = 1 + \varepsilon\cos\theta_i \qquad (26)$$

$$\frac{dH_i}{d\theta} = -\varepsilon\sin\theta_i \qquad (27)$$

M and N being the number of grids in the θ and η directions respectively.

As a solution of equation (20), the pressure at any grid location can be expressed as:

$$P_{i,j} = E_{i,j} + \sqrt{E_{i,j}^2 - F_{i,j}} \qquad (28)$$

Equation (28), when applied to all points of the bearing grid yields a set of simultaneous equations. These equations are solved iteratively using Gauss-Seidel iterative scheme with successive over-relaxation to obtain gas pressure values at all the grid locations. Typical bearing pressure distribution in the circumferential and axial directions is shown in Fig.6 and 7 respectively.

4.2.2 Back face of the pad

The pressure distribution at the back face of the pad is computed by employing finite difference methods. Equation (5) is discretised and expressed as:

$$P_{i,j}^2 - 2 E_{i,j} P_{i,j} - F_{i,j} = 0 \qquad (29)$$

where,

$$E_{i,j} = \frac{(P_{i+1,j} + P_{i-1,j})}{2\overline{D}(\Delta\theta)^2} + \frac{3}{4\overline{D}H_i(\Delta\theta)} \frac{dH}{d\theta}\bigg|_i (P_{i+1,j} - P_{i-1,j})$$
$$+ \left(\frac{r}{L}\right)^2 \frac{(P_{i,j+1} + P_{i,j-1})}{2\overline{D}(\Delta\eta)^2}$$
$$\qquad (30)$$

$$F_{i,j} = \frac{(P_{i+1,j} - P_{i-1,j})^2}{4\overline{D}(\Delta\theta)^2} + \left(\frac{r}{L}\right)^2 \frac{(P_{i,j+1} - P_{i,j-1})^2}{4\overline{D}(\Delta\eta)^2} \qquad (31)$$

$$\Delta\theta = \frac{\theta_3}{2M} \qquad (32)$$

$$\Delta\eta = \frac{1}{2N} \qquad (33)$$

$$\overline{D} = 2\left[\frac{1}{(\Delta\theta)^2} + \left(\frac{r}{L}\right)^2 \frac{1}{(\Delta\eta)^2}\right] \qquad (34)$$

$$\overline{H}_i = 1 - \varepsilon_s \cos\left(\frac{\theta_3}{2} - \theta_i\right) \qquad (35)$$

$$\frac{d\overline{H}_i}{d\theta} = -\varepsilon_s \sin\left(\frac{\theta_3}{2} - \theta_i\right) \qquad (36)$$

From equation (45), the pressure at any grid location is determined from the relation:

$$P_{i,j} = E_{i,j} + \sqrt{E_{i,j}^2 + F_{i,j}} \qquad (37)$$

In a manner akin to the computation of partial arc aerodynamic journal bearing (pad front face), equation (37), when applied to all points of the bearing grid, yields a set of simultaneous equations, which is solved iteratively by using Gauss-Seidel iterative scheme with successive over-relaxation. This gives the gas pressure at all the grid

locations. Numerical integration of the pressure values over the bearing surface gives the back face load capacity.

5. Results

The details of the computation process are given in the computational flow chart as described in Fig. 6.   By following the flow and taking some assumed bearing parameters a MATLAB program is written. This provides pressure characteristics of the bearing for different values of bearing parameters hence an optimized design can be selected.
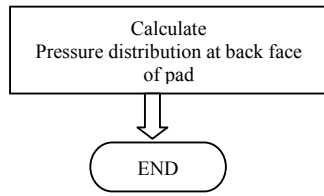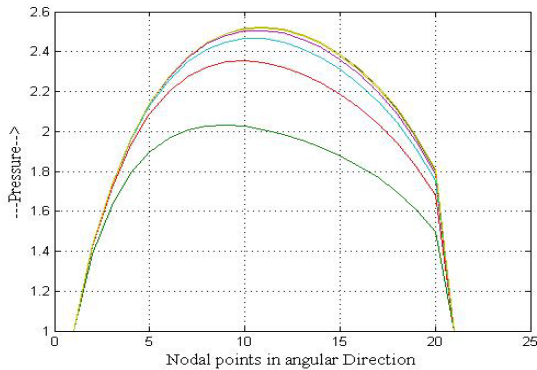
Calculate
Pressure distribution at back face
of pad

END
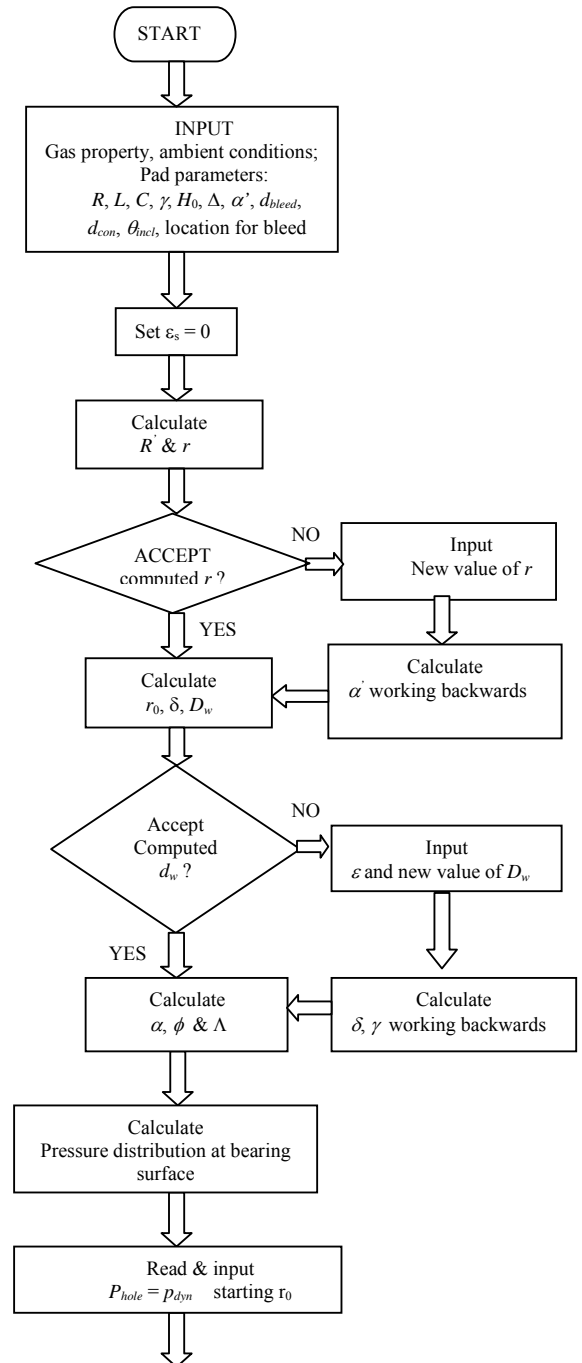
Figure 6: Flow chart for computation process

into 20 divisions. Hence nodal spacing in angular direction is equal to 5.5^o and that in axial direction is equal to 0.9mm. In pad front face, the pressure develops when the shaft rotates and the nature of the pressure distribution developed is shown in figures 7 and 8.The pressure at the edge of pad is equal to atmospheric pressure and at any other point it is more than that along with maximum pressure at some points. The distribution of pressure is such that it should be able to withstand the load.

The pressure distribution obtained for the back face is shown in Fig. 9 and Fig. 10. At the back face the plot of pressure is shown for the half of the back face in axial direction as well as circumferential direction. There is 2 connecting holes are there in the half of the back face through which the pressure transmits to the back face. This is why there are 2 peaks in the plot of the pressure distribution at the back face in both directions. At the other points the pressure variation is slow except at the point of the connecting holes.
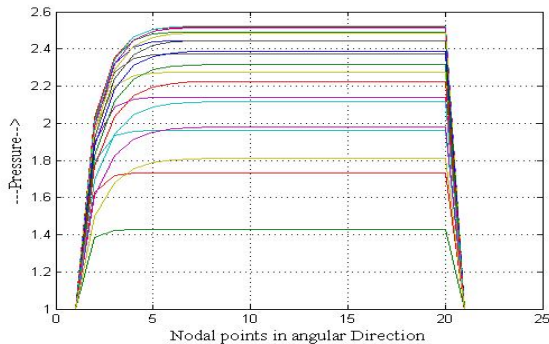
Figure 7: Pressure distribution on the pad front surface along circumferential direction
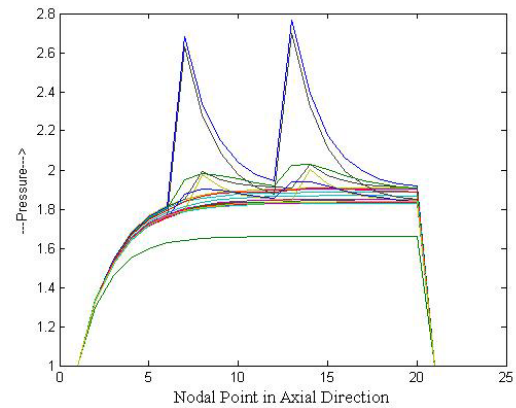
Figure 10: Pressure distribution on the pad back surface along axial direction

6. Conclusion

A theoretical analysis and numerical methods for predicting the pressure characteristics of the pivot less tilting-pad gas bearings are presented. At the same time, the compressible gas-lubricated Reynolds equation is introduced. These are very effective for calculating the dynamic characteristics of gas bearings. The numerical results obtained by means of the partial derivative method and the finite difference method indicates that the bearing parameters have important influence on the dynamic performances of tilting-pad bearing. The abrupt change in the pressure variation at back face of pad is due to the fact that this abrupt change is located at the location of connecting holes where pressure at front face is equal to the pressure at back face.

Figure 8: Pressure distribution on the pad front surface along axial direction

7. References

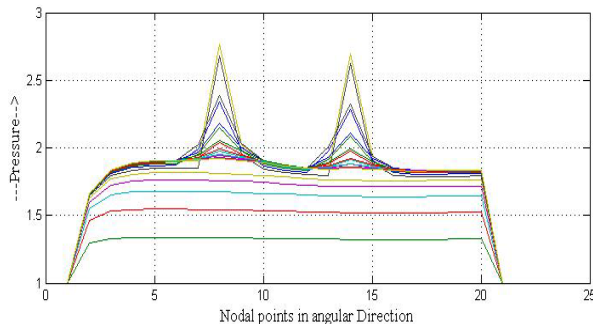1. Michael M. Khonsari and E. Richard Booser."Applied Tribology – Bearing Design and

Figure 9: Pressure distribution on the pad back surface along circumferential direction
For iteration, to determine pressure distribution, the angular dimension as well as the axial dimension is divided

Lubrication" *John Wiley & Sons, New York, USA, 2001, ISBN: 0-471-28302-9*

2. Dr. Majumdar B.C.,"An introduction to tribology of bearings" *S Chand & Company Ltd. ISBN: 8175441828 Pub. 1999*

3. Sixsmith, H. Miniature Cryogenic Expansion Turbines – A Review *Advances in Cryogenic Engineering Plenum Press, New York USA (1984) 29 511-523*

4. Schmidt, C. Gas Bearing Turboexpanders for Cryogenic plants, Paper B1, *6th International Gas Bearing Symposium, University of Southampton (1974)*

5. Chakravarty, A. *Analytical and Experimental Studies on Gas Bearings for Cryogenic Turboexpanders* Ph. D. dissertation, IIT Kharagpur (2000)

6. Yang Lihua, Li Huiguang, Yu Lie,"Dynamic stiffness and damping coefficients of aerodynamic tilting-pad journal bearings" *Tribology International 40 (2007) 1399–1410*

7. Jan Cerma´k, "A non-symmetric discretization formula for the numerical solution of elasto hydrodynamic lubrication circular contact problem.*" Tribology International Vol. 31, No. 12, pp. 761–765, 1998*